Supplementary information

Hierarchical Soot Nanoparticle Self-Assemblies for Enhanced Performance as Sodium-ion Battery Anodes

Yuxiao Cui,‡[a] Chandrasekar M Subramaniyama,‡[a] Lengwan Li,[a,c] Tong Han,[b] Min-A Kang,[a] Jian Li,[a] Luyao Zhao,[a] Xinfeng Wei,[a] Anna J. Svagan*[a] and Mahiar M. Hamedi*[a,c]

a. Royal Institute of Technology (KTH), Dept. of Fibre and Polymer Technology, SE-100 44, Stockholm, Sweden. E-mail: svagan@kth.se, mahiar@kth.se

b. Royal Institute of Technology (KTH), Dept. of Materials Science and Engineering, SE-114 28, Stockholm, Sweden.

c. Wallenberg Wood Science Center (KTH), SE-114 28, Stockholm, Sweden.

‡ Equally contribute to the work.

Experimental details.

Materials

Sodium dodecyl sulfate (SDS), chloroform, and multi-walled carbon nanotubes (MWCNTs) were purchased from Sigma-Aldrich. Candles (Änglamark, Coop) purchased from the local market in Stockholm, Sweden. All the chemicals were analytic grade and used without further purification.

Preparation of the microstructure

Carbon-based soot nanoparticles are collected from burning candles; the soot was collected from the top of the flame using a cleaned glass slide. After depositing the soot particles for 1 minute, the sooth was removed from the glass slide. Next the collected soot underwent heat-treatment for purification and crystallization according to the literature,[4] by annealing at 350 °C for 6 h, firstly, in air and then at 750 °C for 6 h in argon atmosphere. In the next step, 35 mg of heat-treated soot nanoparticles and 1 mg of multi-walled carbon nanotubes (corresponding to 2.8 wt%) were dispersed in 2 mL of chloroform. The suspension, present in a closed vial, was sonicated in a water-bath (BRANSONIC CPX2800H-E) at room temperature for 30 mins to ensure dispersion of the nanoparticles and nanotubes. The obtained hydrophobic phase was poured into

a 20 mL continuous phase consisting of 3.5 mM sodium dodecyl sulfate (SDS) solution in MilliQ-water. Oil-droplets were obtained by mixing the two phases with an IKA T25 digital Ultra Turrax (14000 rpm) for 90 s. The emulsion, present in an open glass vial, was magnetically stirred overnight at 700 rpm, during which the chloroform evaporated. The resulting microparticles, dispersed in MilliQ-water, were dialyzed with deionized water for 3 days to remove excess SDS surfactant, the final suspension contained 0.18 wt% microparticles. The suspension was stored in closed vial at room temperature for further characterizations.

Material characterizations

Scanning-electron-microscopy (SEM) micrographs were obtained using a Hitachi SEM S-4800 (Japan) at an accelerating voltage of 1 kV. The samples were coated with Pt/Pd (60/40) for 10 s at a current of 80 mA using a Cressington 208HR sputter coater. Transmission-electron-microscopy (TEM) micrographs were obtained using a JOEL JEM 2010F (Japan) at 200 kV with 10 Å resolution and processed with the Gatan Micrograph software. X-ray powder diffraction (XRD) spectra were conducted on a PANalytical X'Pert PRO powder diffractometer with Cu K_α irradiation scanned between 10 – 90° at 5°/min scan rate and 0.02° step size. The 2D-WAXD measurement was carried on an Anton Paar's SAXSpoint 2.0 system equipped with a Cu Kα radiation and an Eiger R 1M detector with 75×75 μm pixel size. The sample to detector distance was 77 mm, exposed for 10 minutes and measured with a beam size of 500 μm at RT. Raman spectroscopy was obtained using a Jobin Yvon, HR800 UV with laser 514 nm wavelength. X-ray photoelectron spectroscopy (XPS) was carried out using a PHI 5000 versa probe III scanning XPS microprobe. The survey scan to evaluate the overall composition was carried out in the range 0-1250 eV with a step size of 1 eV. The chemical state of each element within the compound was analyzed through selected region scans with a step size of 0.1 eV. Nitrogen adsorption-desorption isotherms were obtained using a Micromeritics model ASAP 2000 instrument operating at 77 K. The surface area (S_{BET}) was calculated by using the BET equation.[20] The micropore volume ($V_{Micropore}$) and the pore size distributions in the micropore range were determined by the Horvath and Kawazoe (KH) method.[20] The mesopore volume ($V_{Mesopore}$) and the pore size distributions in the mesopore range were determined by calculations

using density-functional-theory (DFT). The total pore volume (TPV) is obtained by adding $V_{Micropore}$ and $V_{Mesopore}$ together.

Electrochemical studies

Electrochemical measurements were done in a half-cell configuration in a typical CR2032 type coin cells using a two-electrode system against Na^+/Na^0. To prepare the slurry, the microparticle suspension was first concentrated (final concentration of ca. 1.8 wt%) by gently blowing it with air to speed up the water rate removal. Then carbon black (Super P, 10 wt %, dry content basis) as a conducting agent, and CMC (10 wt %, dry content basis) as a binder were added into above high concentration carbon microparticle suspension. The final slurry, which contained 8:1:1 of microparticles: CMC: Super P (dry weight composition), was stirred overnight at room temperature. To prepare a slurry with neat soot nanoparticles (instead of microparticles), the same steps, as described above, were used and the final slurry contained 8:1:1 of soot nanoparticles: CMC: Super P (dry weight composition). Each slurry was tape-casted over copper coil using doctor's blade and vacuum dried at 80 °C overnight. The dried electrode was cut into 15 mm diameter disc each weigh ~0.5-0.8 mg cm^{-2}. The electrodes were tested as negative electrode for SIB using CR2032 coin cell in an argon filled glove box maintained at <0.5 ppm H_2O and <0.5 ppm O_2. The cell consisted of as-prepared electrodes as working electrode while sodium metal as counter/reference electrode separated by Whatman G/F grade glass-fibre separator impregnated with 1 M $NaPF_6$ in 1:1 (*v/v*) EC: DEC electrolyte. The cells were tested in a specific galvanostatic current density (mA g^{-1}) between 0.002 – 2 V against sodium. The specific capacity of all cells was calculated based on the weight ratio of active material (soot nanoparticles). Cyclic voltammetry (CV) and electrochemical-impedance-spectroscopy (EIS) were determined using BioLogic (VMP3 instruments, France). CV was scanned at 0.1 mV s^{-1} between 0.002 – 2 mV while EIS obtained using sine wave of amplitude of 5 mV in 0.1 MHz – 10 mHz, frequency range.

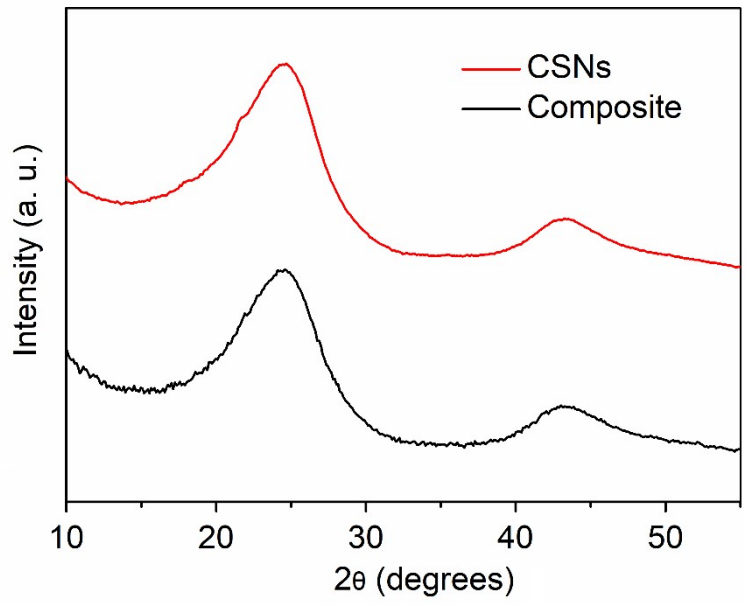

Figure S1 XRD patterns of Carbon-based soot nanoparticles (CSNs) and CSNs/MWCNTs microspheres.

The crystal structure of the composite was analysed using XRD. As seen in Figure S1, the two diffraction peaks of high and low intensity at ~24.5° and ~ 43°, correspond to the (002) and (100) planes, respectively. The broad peak at ~24.5° indicates that the CSNs are amorphous in nature and contains small domains of stacked graphene layers.[1] The peak at ~ 43° confirms the graphitic structure of the crystalline honeycomb lattice carbon.[2, 3] The interlayer spacing (d_{002}) values of the samples, calculated by Bragg's equation had a distance of 0.369 nm, which was slightly larger than CSNs (0.360 nm).

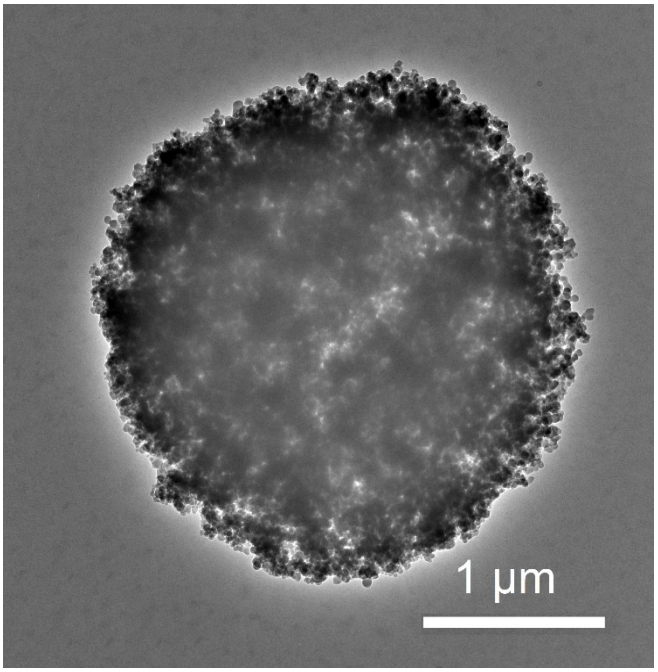

Figure S2 HR-TEM for CSNs/MWCNTs composite.

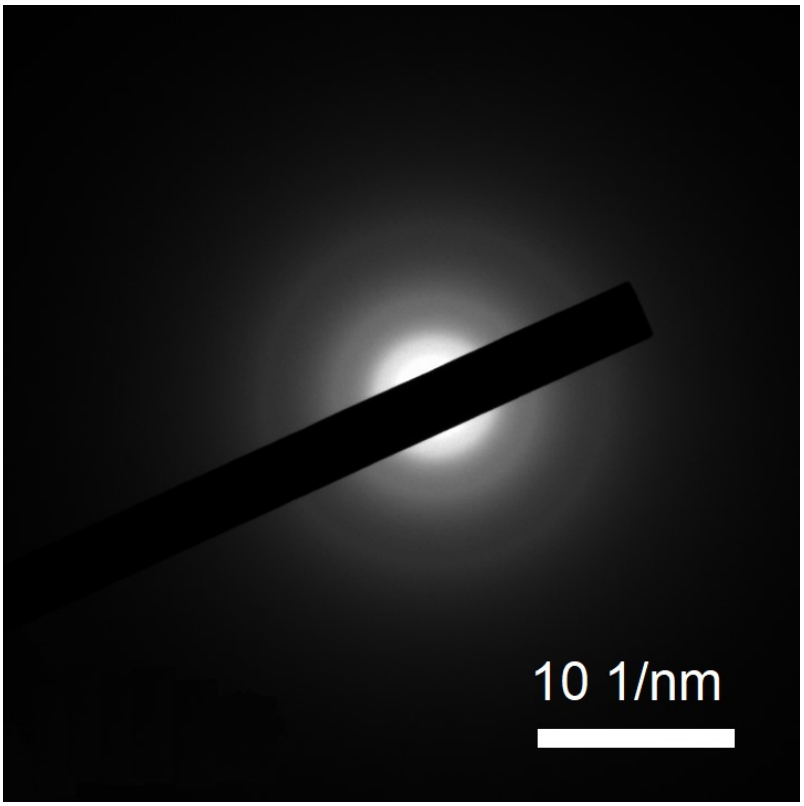

Figure S3 SAED pattern with the corresponding sample in Figure S2.

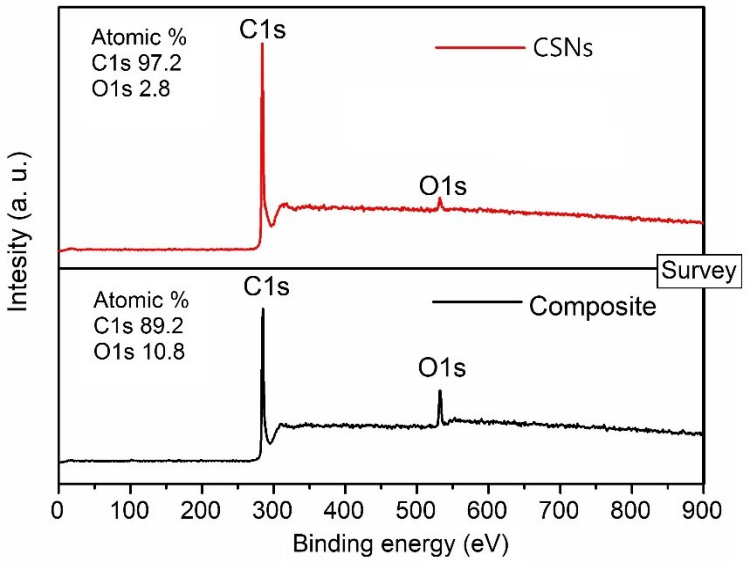

Figure S4 XPS survey spectra for CSNs and CSNs/MWCNTs microparticles.

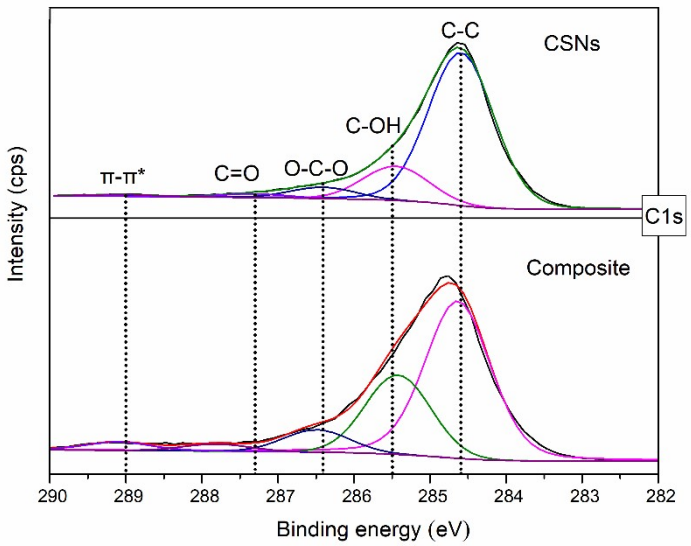

Figure S5 XPS high-resolution spectra of C1s for Carbon-based soot nanoparticles (CSNs) and CSNs/MWCNTs microparticles (composite).

For chemical composition of the CSNs and CSNs/MWCNTs composite, XPS spectra were recorded in Figure S4 and S5. Figure S5 shows the XPS high-resolution spectral of C 1s for the CSNs and

CSNs/MWCNTs composite, which comprises of five components attributable to mixed sp^2/sp^3 C–C bonds, hydroxyl carbon C–OH, O-C-O, carbonyl carbon C=O and π-π^* satellite shake-up peak, the hydroxyl carbon might be due to the adsorption of moisture.[4] In CSNs, the peak at 284.6 eV (76%) was predominant and due to a mixture of sp^2 and sp^3 carbon bonds.[5] In the composite, the intensity of the peak due to mixed sp^2/sp^3 C–C bonds (observed at 284.6 eV) was reduced to 59.5%, with an increase in the two peaks at 286.4 and 287.3 eV, assigned to O-C-O and C=O, respectively. The CSNs also showed less binding energy peak for O1s (XPS survey spectra in Figure S4), which is well in agreement with the C 1s results. The increase in the two peaks at 286.4 and 287.3 eV is due to the introduction of the of MWCNTs in the composite.[6] An additional increase is found for the peak at 289.0 eV (3%) for the composite, compared to the value of 1 % for the CSNs, which is related with the π–π stacking. The presence of π-π* satellite shake-up peak indicates π–π stacking interactions between the layers of graphene carbon skeleton and such interactions indicate improved conductivity.[2]

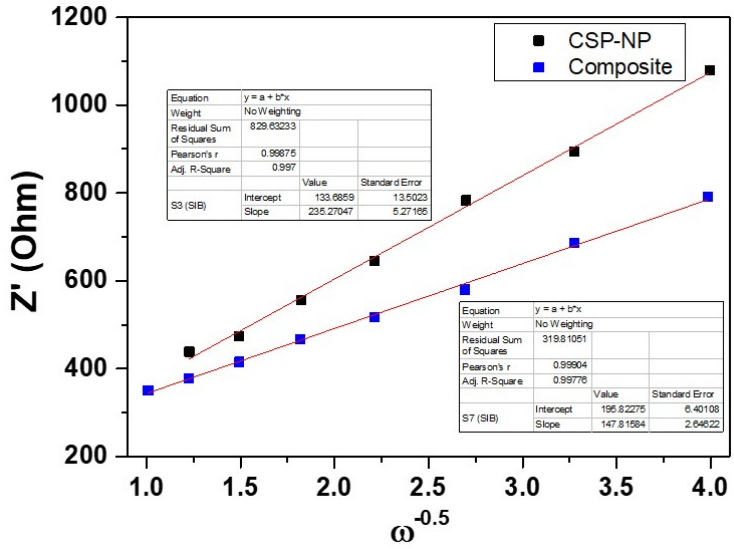

Figure S6 Plot of $\omega^{-0.5}$ vs Z' to determine the slope

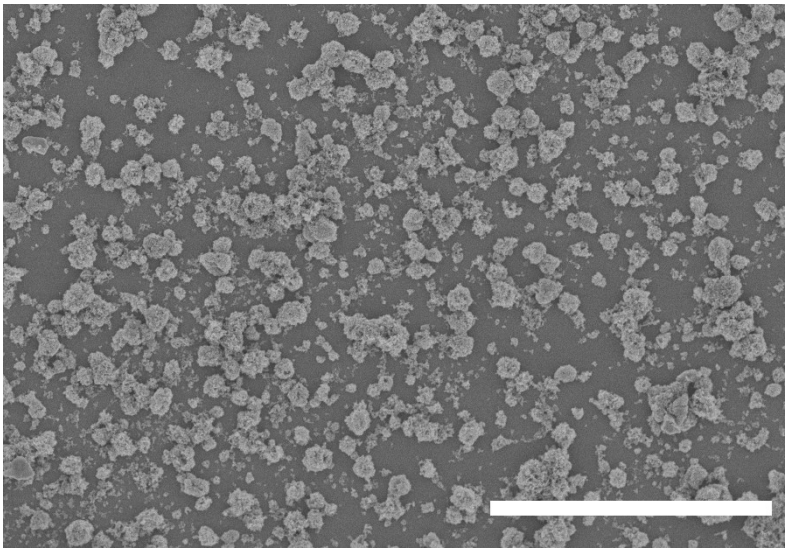

Figure S7 SEM image for the CSNs/MWCNTs composite before cycling (scale bar: 10 μm).

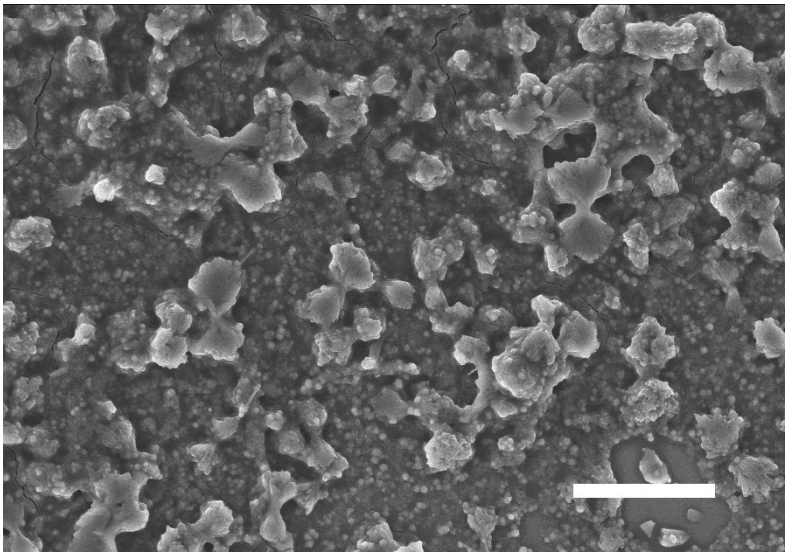

Figure S8 SEM image for the CSNs/MWCNTs composite after cycling (scale bar: 10 μm).

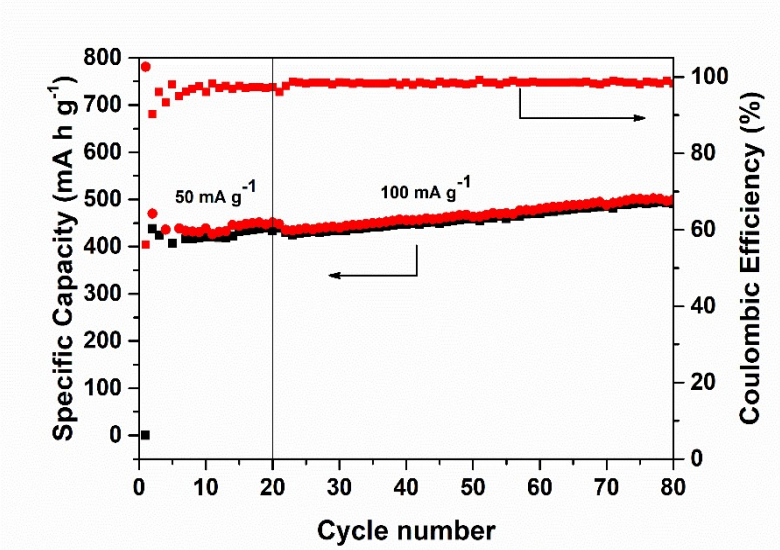

Figure S9 Long cycle stability of composite as lithium anode

Table S1: Comparison of CSNs/MWCNTs microspheres Na-ion battery performance with literature reports

Morphology	**Synthesis Method**	**Potential (V vs Na^+/Na)**	**Current rate ($mA\ g^{-1}$)**	**Initial capacity (Discharge/ Charge) ($mA\ h\ g^{-1}$)**	**Capacity retention ($mA\ h\ g^{-1}$)/ (cycles) $mA\ g^{-1}$**	**Rate test ($mA\ g^{-1}$), (cycle)/ capacity ($mA\ h\ g^{-1}$)**	**Ref.**
Mesoporous microparticles based on Soot nanoparticles and 2.8 wt% MWCNTs	***Water-in-oil emulsion, Ultra Turrax (14 000 rpm) for 90s***	***0.002 – 2***	***50***	***713.3***	***120.8 (500) 500***	***1000 (5) 112.5***	***Present***
Three-dimensional amorphous carbon (3DAC)	3DAC with controlled porous and disordered structures synthesized via a facile NaCl template-assisted method.	0.0 – 3.0	30	280.1	188 (600) 300	1200 (5) 138	[7]
Coal-based amorphous carbon with irregular particles with micron-sized.	Coal-based amorphous carbon synthesized via a simple pulverized coal pyrolysis followed by ball milling, activated with nitric acid and sintered at 600 °C.	0.01 – 2.5	50	342	93 (1000) 500	1000 (5) 90	[8]
Hard carbon sheet-like structure.	Prepared with a short flow process by simply using cherry petals as raw materials.	0.01 – 3.0	20	461.1	131.5 (500) 500	1000 (10) 91.9	[9]
Partially expanded MWCNT (PECNT)	MWCNT prepared by chemical vapor deposition while PECNT prepared by Hummer's method.	0.01 – 2.8	20	1095	120 (100) 200	500 (10) 67	[10]

Hard carbon containing several micron blocks homogenously coated with nanospheres	Hydrothermal treatment route of reed straw-derived hard carbon.	0.0 – 3.0	25	372	252.4 (200) 100	2000 (5) <100	[11]
Amorphous carbon	Ball milling of pitch and phenol-formaldehyde resin	0.01 – 3.0	30	268.3	190 (200) 300	1200 (5)106	[12]
Hard carbon microspheres	To produce the resorcinol formaldehyde resin-derived hard carbon materials by spray drying and carbonization methods.	0.0 – 2.8	25	393	281 (200) 100	1000 (5) 60	[13]
Defective Hard carbon	Biomass derived hard carbon with engineered defective sites using sintering under N2 and CO2 atmosphere.	0.01 – 2.5	25	413	332 (500) 20	1000 (10) 151	[14]
Carbon Nanospheres	Facile chemical bath and hydrothermal process for ZnO nanorod and 0.2 M glucose solution	0.01 - 1.5	250	103	95.2 (100) 250	2000 (5) 65	[15]
Amorphous hard carbon	Hard carbon synthesized by heat-treating microporous phenolic resin at various temperatures	0.0 – 2.0	10	386	-	-	[16]
Hard carbon spheres mix with the carbon nanotubes	Mix the decorated hard carbon spheres and carbon nanotubes, then carbonized at 900 °C in Ar.	0.01 - 3	100	605.8	151.7 (160) 100	3000 (5) 71.7	[17]
Honeycomb-like hard carbon	Carbonization of pine pollen	0.01 – 3.0	100	370.1	203.3 (200) 100	1000 (10) 140.3	[18]
Porous hard carbon	Biomass-derived hard carbon via one-step carbonization of lotus seedpods at 1000-1400 °C.	0.01 – 2.5	50	652.4	161.5 (500) 200	1000 (10) 78.3	[19]

Note: Table compares the Electrochemical performance of present work with the available reported literatures.

(1) Our works shows highest initial discharge capacity of 713.3 mA h g^{-1} compared to others except [10];

(2) The present works outclassed others in term of capacity retention of 120.8 even after 500 cycles at 500 mA g^{-1} while most of the reported literatures shown cycling at low current density (20-300 mA g^{-1}) for a smaller number of cycles;

(3) Our work demonstrated high rate capability of 112.5 mA h g^{-1} at 1000 mA g^{-1} as compared to [8- 13, 15-17, 19].

References

[1] B. Jache, C. Neumann, J. Becker, B. M. Smarsly, P. Adelhelm, Journal of Materials Chemistry 2012, 22, 10787.
[2] M. Kakunuri, C. S. Sharma, Electrochimica Acta 2015, 180, 353.
[3] S. L. Rebelo, A. Guedes, M. E. Szefczyk, A. M. Pereira, J. P. Araújo, C. Freire, Physical Chemistry Chemical Physics 2016, 18, 12784.
[4] R. Kanakaraj, C. Sudakar, Journal of Power Sources 2020, 458, 228064.
[5] Y. Sha, W. Yang, S. Li, L. Yao, H. Li, L. Cheng, H. Yan, W. Cao, J. Tan, RSC advances 2018, 8, 11543.
[6] Z. Wang, P. Zhao, P. Li, S. Li, L. Liao, Y. Luo, Z. Peng, D. He, Y. Cheng, Composites Part B: Engineering 2019, 167, 477.
[7] P. Lu, Y. Sun, H. Xiang, X. Liang, Y. Yu, Advanced Energy Materials 2018, 8, 1702434.
[8] Z. Zhuang, Y. Cui, H. Zhu, Y. Shi, Q. Zhuang, Journal of The Electrochemical Society 2018, 165, A2225.
[9] Z. Zhu, F. Liang, Z. Zhou, X. Zeng, D. Wang, P. Dong, J. Zhao, S. Sun, Y. Zhang, X. Li, Journal of materials chemistry a 2018, 6, 1513.
[10] A. P. Vijaya Kumar Saroja, M. Muruganathan, K. Muthusamy, H. Mizuta, R. Sundara, Nano letters 2018, 18, 5688.
[11] J. Wang, L. Yan, Q. Ren, L. Fan, F. Zhang, Z. Shi, Electrochimica Acta 2018, 291, 188.
[12] Y. Sun, P. Lu, X. Liang, C. Chen, H. Xiang, Journal of Alloys and Compounds 2019, 786, 468.
[13] Q. Zhang, X. Deng, M. Ji, Y. Li, Z. Shi, Ionics 2020, 26, 4523.
[14] T. K. Kumaresan, S. A. Masilamani, K. Raman, S. Z. Karazhanov, R. Subashchandrabose, Electrochimica Acta 2021, 368, 137574.
[15] W. Tang, J. Wu, X. Wang, X. Xia, J. Tu, Green Energy & Environment 2018, 3, 50.
[16] A. Kamiyama, K. Kubota, T. Nakano, S. Fujimura, S. Shiraishi, H. Tsukada, S. Komaba, ACS Applied Energy Materials 2019, 3, 135.
[17] L. Suo, J. Zhu, X. Shen, Y. Wang, X. Han, Z. Chen, Y. Li, Y. Liu, D. Wang, Y. Ma, Carbon 2019, 151, 1.
[18] Y. Zhang, X. Li, P. Dong, G. Wu, J. Xiao, X. Zeng, Y. Zhang, X. Sun, ACS applied materials & interfaces 2018, 10, 42796.
[19] F. Wu, M. Zhang, Y. Bai, X. Wang, R. Dong, C. Wu, ACS applied materials & interfaces 2019, 11, 12554.
[20] R. Bardestani, G. S. Patience, S. Kaliaguine, The Canadian Journal of Chemical Engineering 2019, 97, 2781.